The Egyptian Journal of Remote Sensing and Space Sciences (2016) 19, 49–60

HOSTED BY

ELSEVIER

National Authority for Remote Sensing and Space Sciences

The Egyptian Journal of Remote Sensing and Space Sciences

www.elsevier.com/locate/ejrs
www.sciencedirect.com

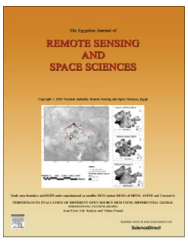

RESEARCH PAPER

Hydrogeological activity of lineaments in Yaoundé Cameroon region using remote sensing and GIS techniques

William Teikeu Assatse [a], Philippe Njandjock Nouck [a,*], Charles Tabod Tabod [a,c], Joseph Martial Akame [d], Georges Nshagali Biringanine [a,b]

[a] *Laboratory of Geophysic, University of Yaoundé I, 812 Yaoundé, Cameroon*
[b] *Department of Geology, Official University of Bukavu, 435 Cyangugu, Rwanda*
[c] *Department of Physic, University of Bamenda, 39 Bambili, Cameroon*
[d] *Laboratory of Petrology and Structural Geology, University of Yaoundé I, 812 Yaoundé, Cameroon*

Received 17 February 2015; revised 22 December 2015; accepted 28 December 2015
Available online 21 January 2016

KEYWORDS

Geostatistics;
Lineaments;
Remote sensing;
Crystalline basement

Abstract Though Yaoundé zone is characterized by abundant rains, access to safe drinking water becomes a difficult activity, because of climate change and pollution caused by human activities. Lineament zones on the earth's surface are important elements in understanding the dynamics of the subsurface fluid flow. However, good exposures of these features are always lacking in some areas around Yaoundé, characterized by thick alteration. During field surveys these conditions, in many cases, hinder the proper characterization of such features. Therefore, an approach that identifies the regional lineaments on remote-sensing images (Landsat Thematic Mapper and shaded digital terrain models), with its large scale synoptic coverage, could be promising. This paper aims to the structural organization of lineament network in the crystalline basement of Yaoundé from remote sensing data and characterize them by statistical and geostatistical techniques. The results were validated on the basis of the geological maps, the hydrogeological maps and the outcrop data. Statistical analysis of the lineaments network shows a distribution along the N0–10, N20–30, N40–60 and N140–150. The correlation between the productivity of high yield wells and the closest lineament confirms that these lineaments are surface traces of regional discontinuities and act as main groundwater flow paths.

1. Introduction

In the Yaoundé crystalline basement area, despite strong rainfall, the groundwater wells for feeding populations are characterized by very low water flow rates which are sometimes

* Corresponding author.
E-mail address: pnnouck@yahoo.com (P. Njandjock Nouck).
Peer review under responsibility of National Authority for Remote Sensing and Space Sciences.

http://dx.doi.org/10.1016/j.ejrs.2015.12.006

unsuccessful (Teikeu et al., 2012a,b). The remote sensing techniques have opened a new area in the field of applied geology (Farina et al., 2005). Due to its efficiency in detecting geological structures (e.g., lineaments), the technique of digital image processing proved that, remote sensing is a useful tool for mapping minerals. Other techniques were also applied to emphasize the role of remote sensing in detecting lineaments (Corgne et al., 2010). The availability of multi-spectral and high-resolution data as well as the advanced capabilities of digital image processing techniques in generating enhanced and interpretable images further enlarged the potential of remote sensing in delineating the geological structures in detail and with better accuracy (Akame et al., 2014; Masoud and Koike, 2006). Many geological studies have employed Shuttle Radar Topography Mission (SRTM) and Landsat Thematic Mapper (LTM) to discriminate the various lithology, lineaments and minerals using hyperspectral laboratory (Akame et al., 2013; Tarek, 2013; Koike et al., 1998). Subsequent studies confirmed their benefit for lineament mapping using the remote sensing data and GIS techniques (Singh et al., 2013; Rashid et al., 2012). The objective of this work is to characterize and analyze the spatial organization of lineaments from SRTM and LTM data using statistical and geostatistical techniques, to determine their role in groundwater flow in bedrock aquifers in the Yaoundé region.

2. Description of the study area

The study area is located in the Center of Cameroon, between latitudes 3° and 5° N and longitudes 11° and 13° E (Fig. 1). It is a slightly undulating vast forest region with thick lateritic soil developed on a Neoproterozoic basement (Ngon-Ngon et al., 2009; Tanawa et al., 2002). It has an arborescent hydrographic network, with the Mefou and Mfoundi being main rivers (Fig. 1). This hydrographic network has developed flat valleys with different widths ranging from 50 to 150 m (Ngon-Ngon et al., 2009). The geomorphology data are derived from the DEM. Geomorphology is influenced by lithology and structure of the underlying formations and plays a pivotal role in the occurrence and distribution of groundwater (Fashae et al., 2014). Geomorphological mapping (Fig. 2) involved the identification and characterization of various landforms comprising mountainous massifs (> 800 m), the Yaoundé plateau (~750 m) and low swampy valleys (< 700 m).

The climate is particularly hot and humid with two rainy seasons (mid-March–mid-June and mid-August–mid-November) and two dry seasons (mid-November–mid-March and mid-June–mid-August).

The annual average rainfall calculated for the 1984–2012 period is 1626 mm/year and Average evaporation (EVT) of 948 mm/year (Fig. 3). Average annual temperature rate is 24 °C.

Geologically, the Neoproterozoic basement (Fig. 4) is composed of gneisses and migmatites (Mvondo et al., 2003; Ngnotué et al., 2000; Nzenti, 1998). Meta sedimentary rocks are the most abundant outcrop along the beds of some rivers. The structural features in migmatites and basement gneisses were described by Mvondo et al. (2003) and Nzenti et al. (1988). They suggest that, the study area has undergone three phases of ductile deformation, mainly corresponding to E–W to NW–SE compressions (D1 and D3) alternating with a N–S to NE–SW extensive phase (D2). The initial phase D1 is associated with prograde metamorphism culminating at high pressure granulite conditions. On the other hand, the D2 phase represents the decompression phase. It is probably associated to intense magmatic activity, the large-scale foliation and formation of gneiss domes transposing D1 phase to form flat regional structures. A third non-penetrative and essentially

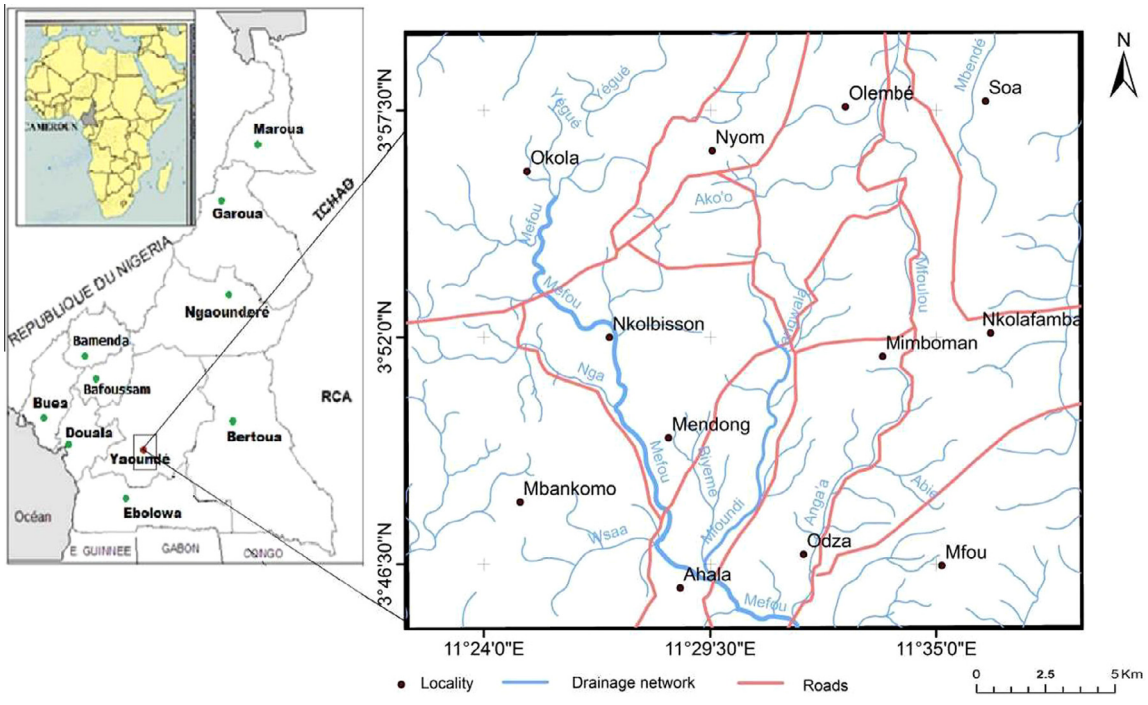

Figure 1 Location map of the study area.

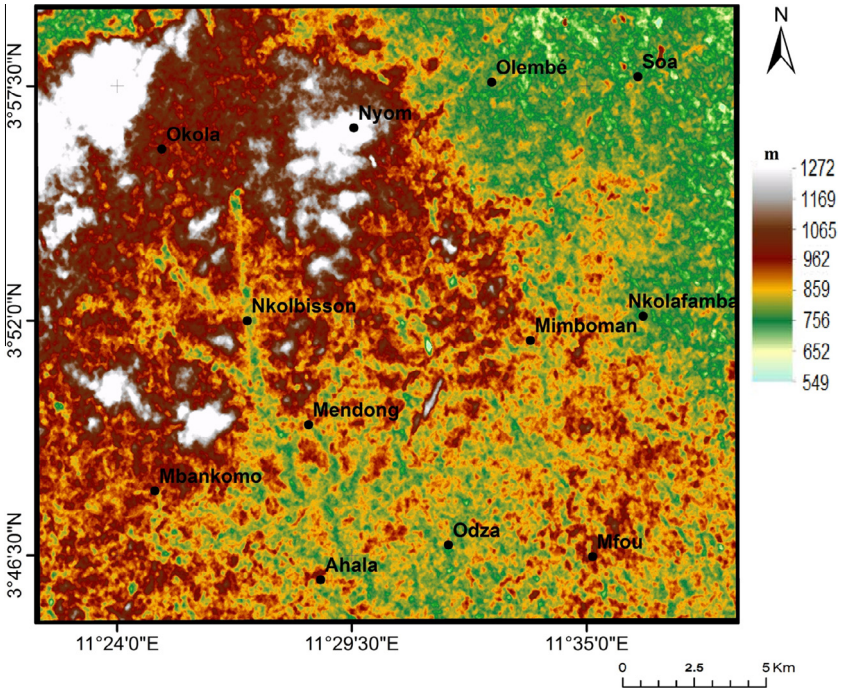

Figure 2 Geomorphology map of the study area.

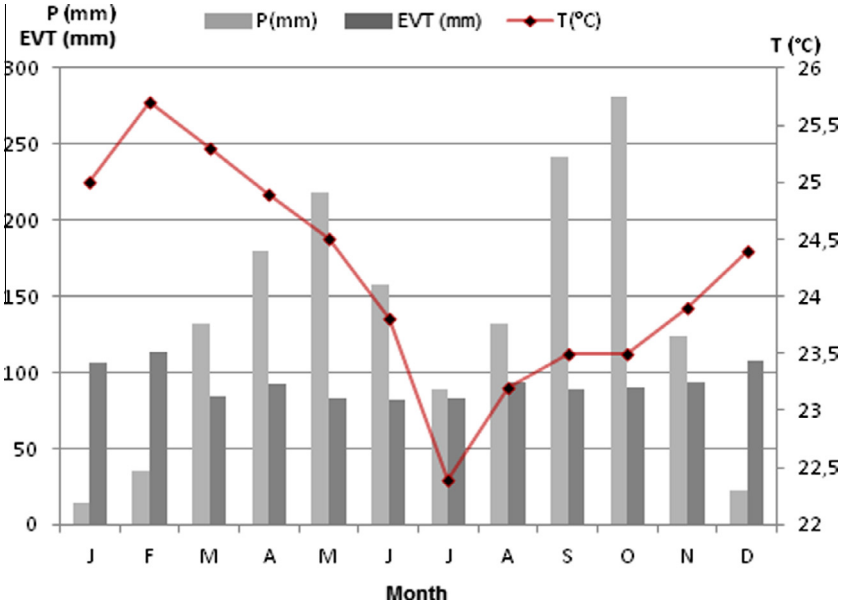

Figure 3 Trend of mean monthly rainfall, temperature and evaporation within the study area.

brittle D3 phase comprises the joint veins, fractures and faults. These deformation phases are responsible for the topographic shape that strongly influences the hydrography. Fragmentation of relief and hydrography is closely dependent. Recently, Owona et al. (2011), Mvondo Ondoa (2009) and Mvondo et al. (2007) highlighted a fourth deformation phase D4, plicative and attributed to lateral flows subsequent to diachronic crustal extensions.

3. Materials and methods

3.1. Materials

In this study, several types of data were used. They include topographic and geological map of the study area at 1/5,00,000 scale from the Institute of Geological and Mining Research of Cameroon, and a hydrographic map, a digital

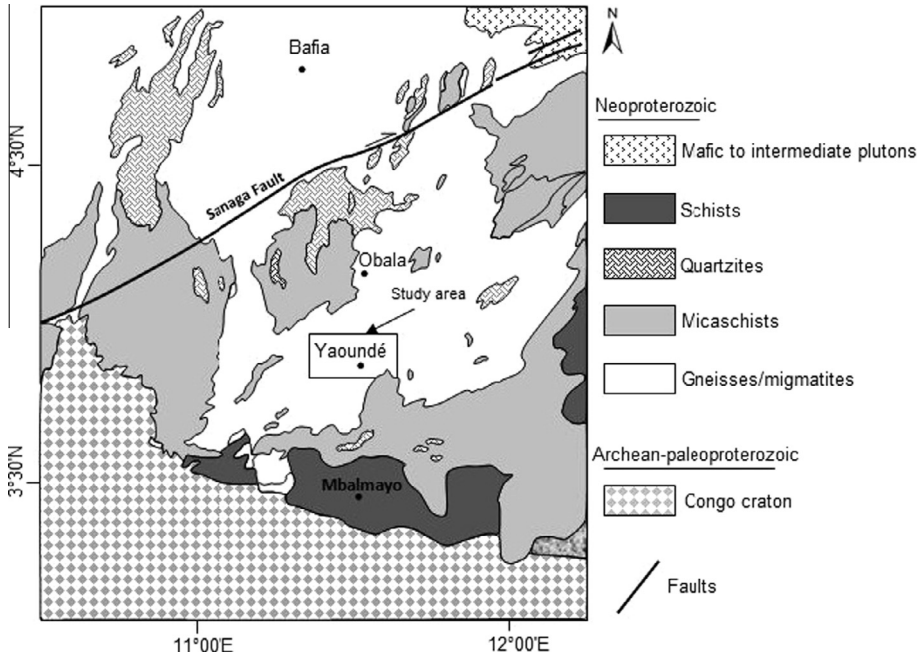

Figure 4 Geological map of study area (Champetier De Ribes and Aubargue, 1956).

elevation model (DEM) extracted from Shuttle Radar Topography Mission (SRTM) and Landsat Thematic Mapper (LTM) image (Scene 185-57) acquired on 02/02/1988 corresponding to the long dry season. These data were provided by the National Institute of Cartography of Cameroon. The DEM is a digital representation of the earth surface terrain that could be beneficially integrated in the structural geology for the identification of lineaments and fracture systems that may represent the surface expression of geological structures (Abou El-Magd et al., 2010; Michaela et al., 2006). In this topic, the results of DEM interpretation were combined by other remote sensing data such as optical multi-spectral data (Landsat TM). The geological outcropping of the study area has been analyzed in some sites to confirm the result of lineament analysis obtained from remote sensing data.

The digital image processing, thematic mapping, extraction lengths and directions of lineament were obtained using the Erdas imagine 2011 and ArcGIS 10.1 software, respectively. Statistical and geostatistical analysis of network lineaments were performed by XLSTAT software and geostatistics program (Autogrig) developed by the Geophysical Laboratory of the University of Yaounde I in a Matlab platform, respectively.

3.2. Methodology

The Landsat image and DEM of the study area and its surrounding were geometrically registered using GIS software with scanned topographic map of the study area (with a scale of 1:5,00,000) and geodetically transformed into the Universal Transverse Mercator (UTM) zones 32.

For the first image, two image-processing steps were proposed to increase the sharpness of the Landsat image, clarify the features and obtain more reliable information. The first step concerned the image sharpening and was applied to the Landsat image for lineament analysis and lithological mapping (Fig. 5a). The Principal Components Analysis (PCA) has been performed on bands 1, 2, 3, 4, 5, 6 and 7 of the TM image. PCA is used in order to reduce spectral redundancy in the Landsat TM data and to represent entire spectral information in a single RGB color combination image (PC1–PC2–PC3). To improve the contrast of images, some information has been enhanced with the application of color composition on TM bands 4, 5 and 7. The second step concerned application of directional 7×7 Sobel filters in the NS, EW, NE–SW and NW–SE direction; and the Yesou et al. (1993) gradient to channels $TM_{7\text{-}5\text{-}4}$, TM5/TM4 and PC1 help to enhance image discontinuities corresponding to structural lineaments. This image had a spatial resolution of 30 m which enables the delineation of the geological lineaments in the study area.

The second image used for the interpretation is the SRTM DEM having spatial resolution of 90 m. DEM data extracted from SRTM data were used to recognize and extract geological lineaments by calculating and interpreting DEM derivatives, including shaded relief maps. The shaded relief map was calculated from a gray scale using an azimuth direction and input sun angles of 0, 45, 90, 135, 180, 225, 270 and 315 (Fig. 5b).

The processing and filtering have accentuated and facilitated the detection of lineament in the images, thus allowing their extraction by a simple visual observation.

Lineaments that show little relationship to topographic features and a Strong relationship to anthropogenic features are considered to be formed by anthropogenic factors. To identify lineaments within the lineament map which were caused by infrastructure, digitized road and the topographic maps were superimposed over the final lineament maps using ArcGIS 10.1.

3.3. Statistical and geostatistical analysis methods

The statistical approach of the geometric parameters (directions and lengths) of lineaments is required to describe the

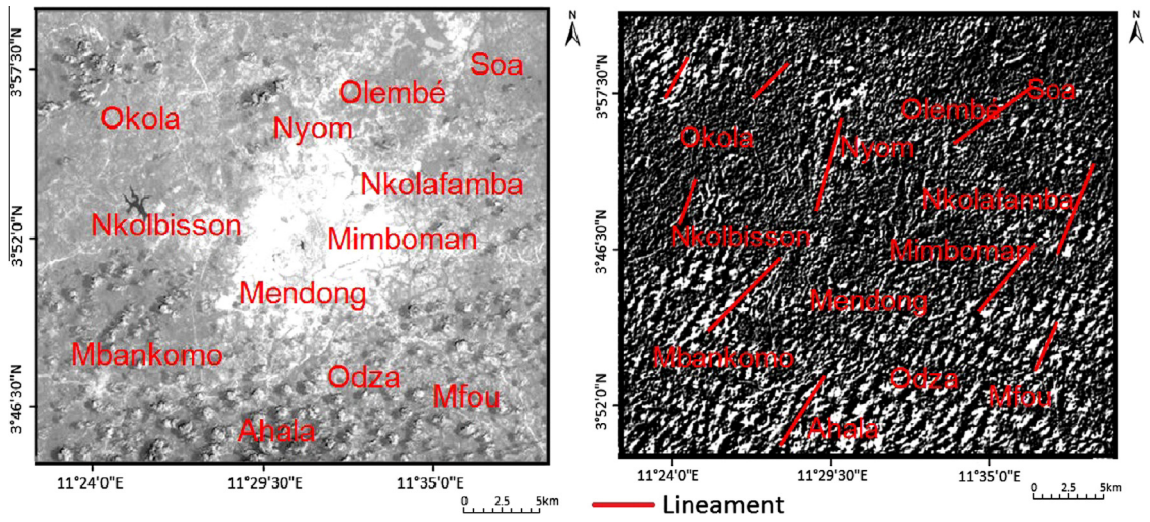

Figure 5a Lineament map from Landsat TM.

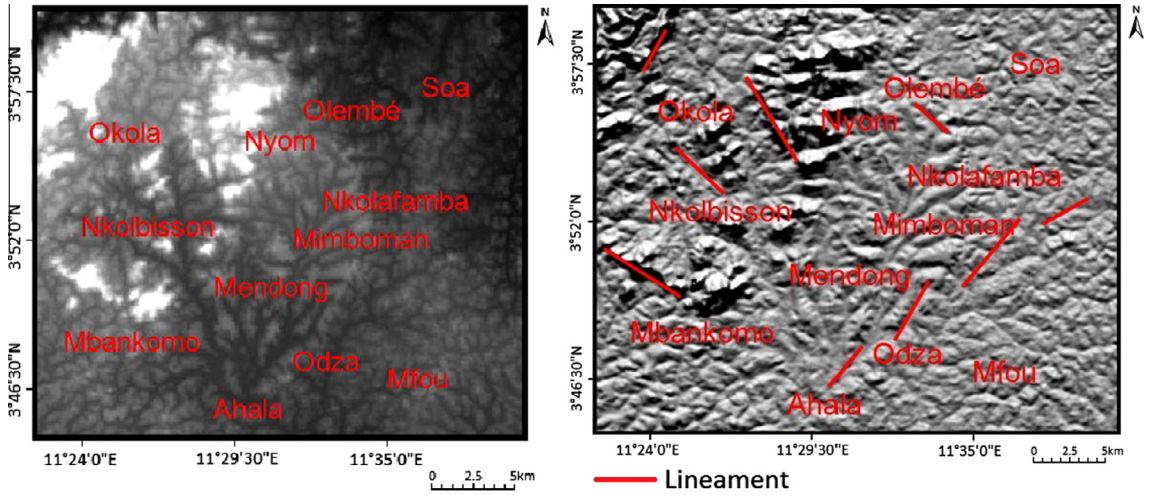

Figure 5b Lineament map from SRTM data.

structure of a region. The processing of the orientation of lineaments, done on homogeneous geographical area if needed, simply produces a directional diagram which shows the distribution of fractures by classes of 10°. The length parameter is analyzed using a frequency histogram which is adjusted by many statistical models (exponential, gamma, log-normal, and power). The lineament, spatial phenomenon may be subjected to geostatistical analysis. The geostatistical analysis is based on the regionalized variables theory (Goovaerts, 2000), which enables one to quantify the spatial variability of the phenomenon based on the values observed at different measurement sites and depending on the distance between them (Njandjock et al., 2013). Experimentally, its mathematical tool is the variogram γ (h) given by Eq. (1)

$$\gamma(h) = \frac{1}{2N}\sum_{i=1}^{N(h)}[Z(x_i) - Z(x_i + h)]^2 \quad (1)$$

where $Z(x)$ and $Z(x_i + h)$ are the values of the variable Z at the position x_i and $x_i + h$, respectively, $N(h)$ is the number of pairs which are distant by h.

Ideally, for a point of the experimental variogram to be considered as representative, it is necessary that $N(h) \geqslant 30$. To these point values, an acceptable theoretical model of variogram is adjusted. The main accepted models are linear, spherical, exponential, cubic, Gaussian and logarithmic. The description of these models depends on a number of quantization parameters such as range, bearing and nugget effect.

The choice of the variogram model is guided by the degree of fitness between the experimental and theoretical values (Meli'i et al., 2013). This degree of fitness can be evaluated by the root mean square error (RMS) given by Eq. (2):

$$RMS = \left[\frac{1}{N}\sum_{i=1}^{N}((Z^*(x_i) - Z(x_i))^2\right]^{1/2} \quad (2)$$

where $Z^*(x_i)$ and $Z(x_i)$ are the theoretical and experimental values for the measurement points x_i, respectively.

4. Results and discussion

4.1. Mapping of structural lineaments network

The detailed map from the manual extraction of lineaments (Fig. 6) was carried out through the application of the different processing techniques.

The validation of the detailed map of lineaments is a very important step that determines the use of the map for future hydrogeological surveys. It allows assigning the value of fracture to all the selected lineaments (Chaabouni et al., 2012). This important step was made from data obtained after lineament operation of photo-geological, topographical, hydrographical and measures outcrop study area maps (Fig. 7).

4.2. Statistical analysis of the lineament network

The total length of lineaments mapped is 1883.8 km. The lengths of lineaments mapped can be grouped into three main classes (Fig. 8). A main class (70.6%) which includes lineaments whose lengths are between 0.2 km and 1.9 km, followed by a smaller class of fracture (27.8%) have lengths between 2.0 km and 4.9 km and finally, a minority class (1.5%) whose lengths are beyond 4.9 km.

The lineaments were adjusted with a non parametric statistic test. The results of the adjustment tests at 1% significant level by different laws are shown in Table 1.

These laws (log-normal, gamma and exponential) do not statistically permit the description of lineaments' length, notably at the level of small values. We then, tried to model this distribution by a power law. Fig. 9 shows a logarithmic diagram of empirical distribution of the length with part of 0.22 km. On this graph, it is only the part of the curve found between 1.13 km and 6.79 km that presents a comportment which we access to be linear. We therefore adjusted on this part the power law expression according to Eq. (3).

$$n(L) = 140.4L^{-2.235} \tag{3}$$

The residual coefficient R^2 is low (0.92) and the adjustment tests are not conclusive. Below 1.02 km, this power law is not respected: the slope put into evidence the resolution limits which exclude 27% of cumulated lineaments' length compared to the total. Characteristic exposure of the power law is equal to 2.24 and far away from value 3. This value is compatible with the literature data generally comprising between 1 and 3, which can vary from one fracture network to another as testified by Lasm and Razack (2001), Bodin and Razack (1999). The α exhibition thus fits the proportion of large or great fractures than the small ones. The variations of α define in particular the different developmental stages or the maturity of fracture networks (Lasm et al., 2008; Chilès and de Marsily, 1993; Chilès et al., 1992). This power law points out that, the fracture networks of the Yaoundé region would have attended an advanced developmental stage.

4.3. Geostatistical analysis of the lineaments

The adjustment of experimental variograms to theoretical models is an important step in the identification and interpretation of the regionalization parameters (Moukana and Koike, 2008). For each variogram model, we note the existence of the

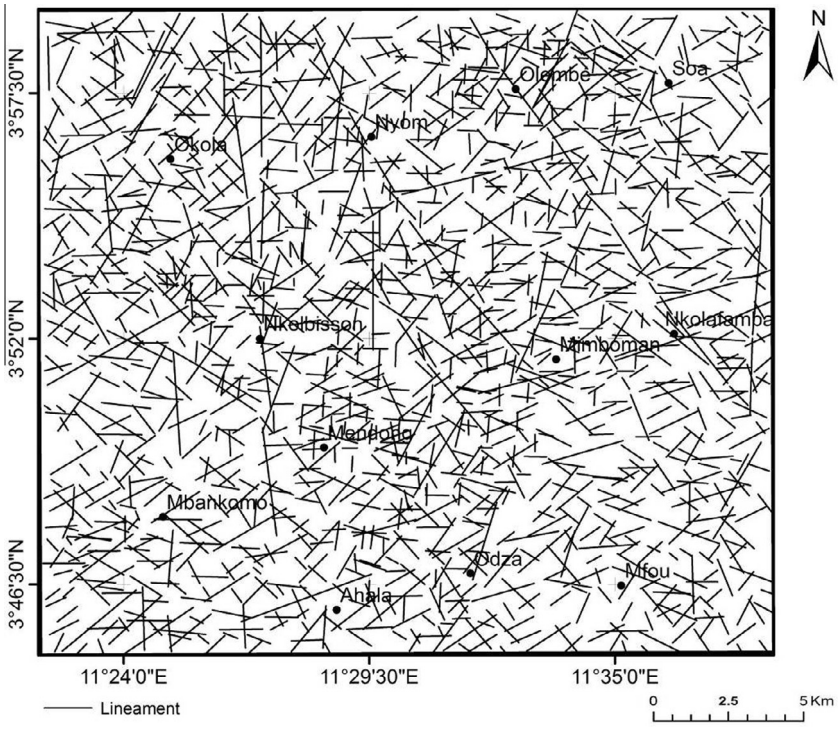

Figure 6 Detailed map of lineaments of study area.

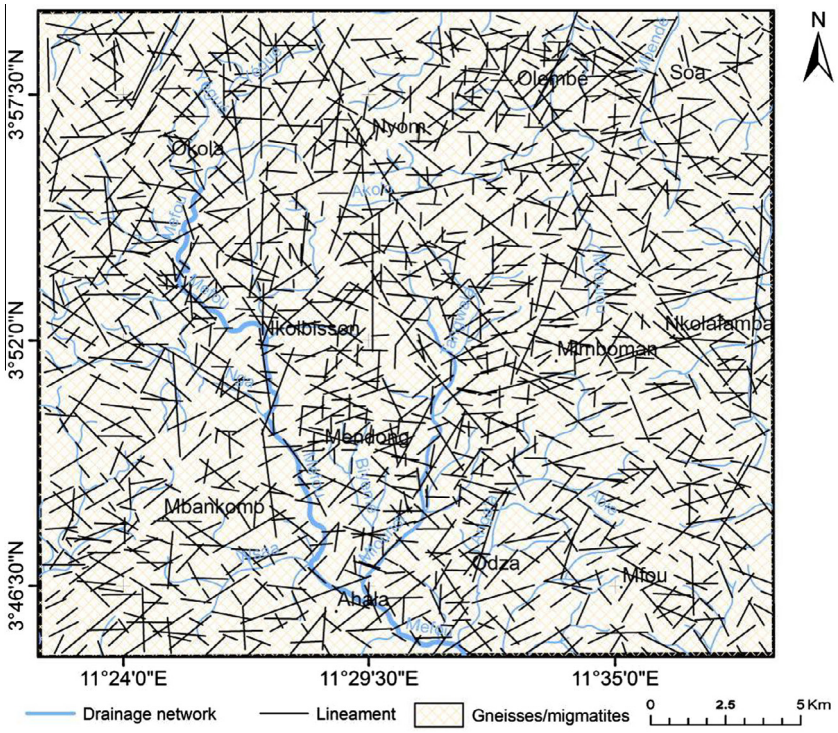

Figure 7 Combination of remote sensing lineament and hydrogeological map of study area.

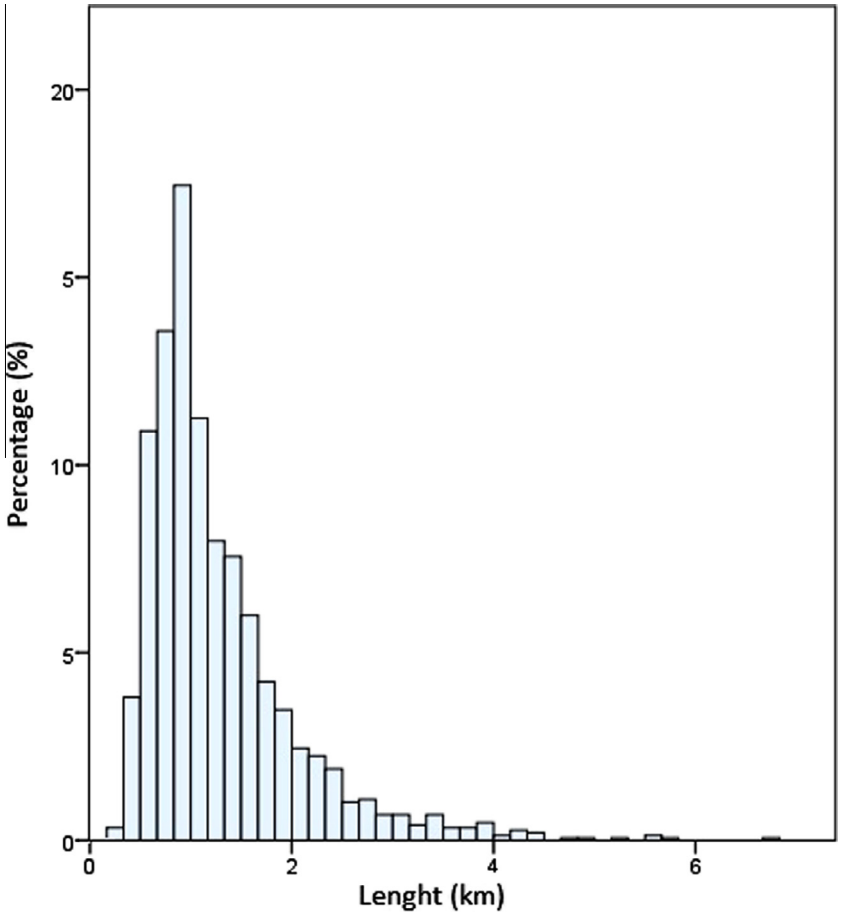

Figure 8 Lineaments' length histogram.

Table 1 Adjustment tests χ^2 and K–S (Kolmogorov–Smirnov) of the lineaments' length.

Law of distribution and its parameters	Calculated χ^2	Degree of freedom	Theoretical χ^2 (1%)	Test of K–S $p < 0.01$
Log-normal ($\mu = 1.11$; $\sigma = 0.26$)	45.898	6	16.812	0.049
Gamma ($\varepsilon = 0.34$; $\beta = 3.71$)	180.096	5	15.086	0.075
Exponential ($\lambda = 0.78$)	855.816	12	26.217	0.281

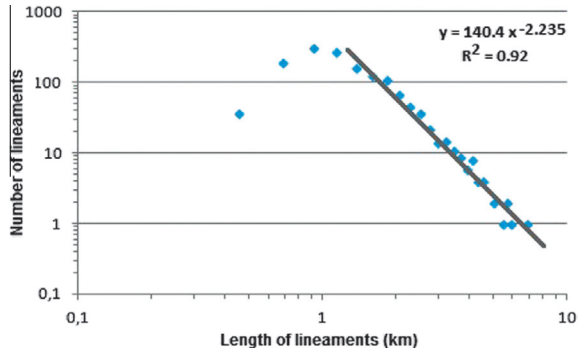

Figure 9 Power-law graph of the lineament length.

following parameters: the range "a" mean separation distance of two points beyond which the property values become statistically independent, the sill ($C + C_O$) value at which the variogram stabilizes. Among models, only the spherical variogram model has been deemed admissible because its RMS values (Table 2) are lowest.

Its general expression is given by the Eq. (4):

$$\gamma(h) = \begin{cases} C_o + C\left[\frac{3}{2}\left(\frac{h}{a}\right) - \frac{1}{2}\left(\frac{h}{a}\right)^3\right] & h < a \\ C_o + C & h \geqslant a \end{cases} \quad (4)$$

The cumulative length variogram of lineaments in the main directions N–S, E–W, NW–SE and NE–SW are adjusted to the spherical model (Fig. 10a–d) and summarized in Table 3.

The structural distance of lineament's families along these directions are: $a_{\text{N–S}} = 5$ km, $a_{\text{E–W}} = 11$ km and $a_{\text{NW–SE}} = 9$ km and $a_{\text{NE–SW}} = 4$ km, respectively.

The modeling relations of these variograms are represented by the Eqs. (5)–(8):

$$\gamma_{\text{N–S}}(h) = \begin{cases} 1.2 + 6.4\left[\frac{3}{2}\left(\frac{h}{5}\right) - \frac{1}{2}\left(\frac{h}{5}\right)^3\right] & h < 5 \text{ km} \\ 1.2 + 6.4 & h \geqslant 5 \text{ km} \end{cases} \quad (5)$$

$$\gamma_{\text{E–W}}(h) = \begin{cases} 0.4 + 1.3\left[\frac{3}{2}\left(\frac{h}{11}\right) - \frac{1}{2}\left(\frac{h}{11}\right)^3\right] & h < 11 \text{ km} \\ 0.4 + 1.3 & h \geqslant 5 \text{ km} \end{cases} \quad (6)$$

$$\gamma_{\text{NW–SE}}(h) = \begin{cases} 3.1 + 2.3\left[\frac{3}{2}\left(\frac{h}{9}\right) - \frac{1}{2}\left(\frac{h}{9}\right)^3\right] & h < 9 \text{ km} \\ 3.1 + 2.3 & h \geqslant 9 \text{ km} \end{cases} \quad (7)$$

$$\gamma_{\text{NE–SW}}(h) = \begin{cases} 6.0 + 1.3\left[\frac{3}{2}\left(\frac{h}{4}\right) - \frac{1}{2}\left(\frac{h}{4}\right)^3\right] & h < 4 \text{ km} \\ 6.0 + 1.3 & h \geqslant 4 \text{ km} \end{cases} \quad (8)$$

These range values are different from a statistical point of view, indicating that lineaments behave differently along the different spatial directions (Lasm et al., 2008). Beyond this distance, there is no correlation between the different points.

The variogram of global lineaments shows a particular behavior characterized by four sill levels. This may be an indication of several interlocking structures at different scales (Lasm et al., 2008). The global lineament in the total length is therefore characterized by a quadruple regionalization. Regionalization parameters are adjusted to spherical models (Fig. 11). The equations of the four elementary variograms are given by the expressions (9)–(12):

$$\gamma_1(h) = \begin{cases} 0.3 + 2.8\left[\frac{3}{2}\left(\frac{h}{1.6}\right) - \frac{1}{2}\left(\frac{h}{1.6}\right)^3\right] & h < 1.6 \text{ km} \\ 0.3 + 2.8 & h \geqslant 1.6 \text{ km} \end{cases} \quad (9)$$

$$\gamma_2(h) = \begin{cases} 4.5\left[\frac{3}{2}\left(\frac{h}{3.5}\right) - \frac{1}{2}\left(\frac{h}{3.5}\right)^3\right] & h < 3.5 \text{ km} \\ 4.5 & h \geqslant 3.5 \text{ km} \end{cases} \quad (10)$$

$$\gamma_3(h) = \begin{cases} 5.6\left[\frac{3}{2}\left(\frac{h}{5.8}\right) - \frac{1}{2}\left(\frac{h}{5.8}\right)^3\right] & h < 5.8 \text{ km} \\ 5.6 & h \geqslant 5.8 \text{ km} \end{cases} \quad (11)$$

$$\gamma_4(h) = \begin{cases} 6.8\left[\frac{3}{2}\left(\frac{h}{9.6}\right) - \frac{1}{2}\left(\frac{h}{9.6}\right)^3\right] & h < 9.6 \text{ km} \\ 6.8 & h \geqslant 9.6 \text{ km} \end{cases} \quad (12)$$

The modeled global variogram of lineaments (Eq. (13)) corresponds to the sum of elementary variograms

$$\gamma(h) = \gamma_1(h) + \gamma_2(h) + \gamma_3(h) + \gamma_4(h) \quad (13)$$

The nugget effect represents 9.67% of the lineaments total dispersion in all directions; this value is 15.79%, 23.53%, 57.40% and 0.82% for N–S, E–W, NW–SE and NE–SW group of lineaments, respectively. In general, these variograms exhibit a very low dispersion, except along the NE–SW direction. This

Table 2 RMS misfit to theoretical model.

Family of lineament	N–S		E–W		NW–SE		NE–SW		All azimuth	
Variogram model	sph	exp	sph	exp	sph	exp	sph	exp	sph	exp
Root mean square (RMS)	2.4	4.1	2.2	3.0	2.4	3.3	2.6	4.1	1.7	2

Where sph and exp are the spherical and exponential variogram model, respectively.

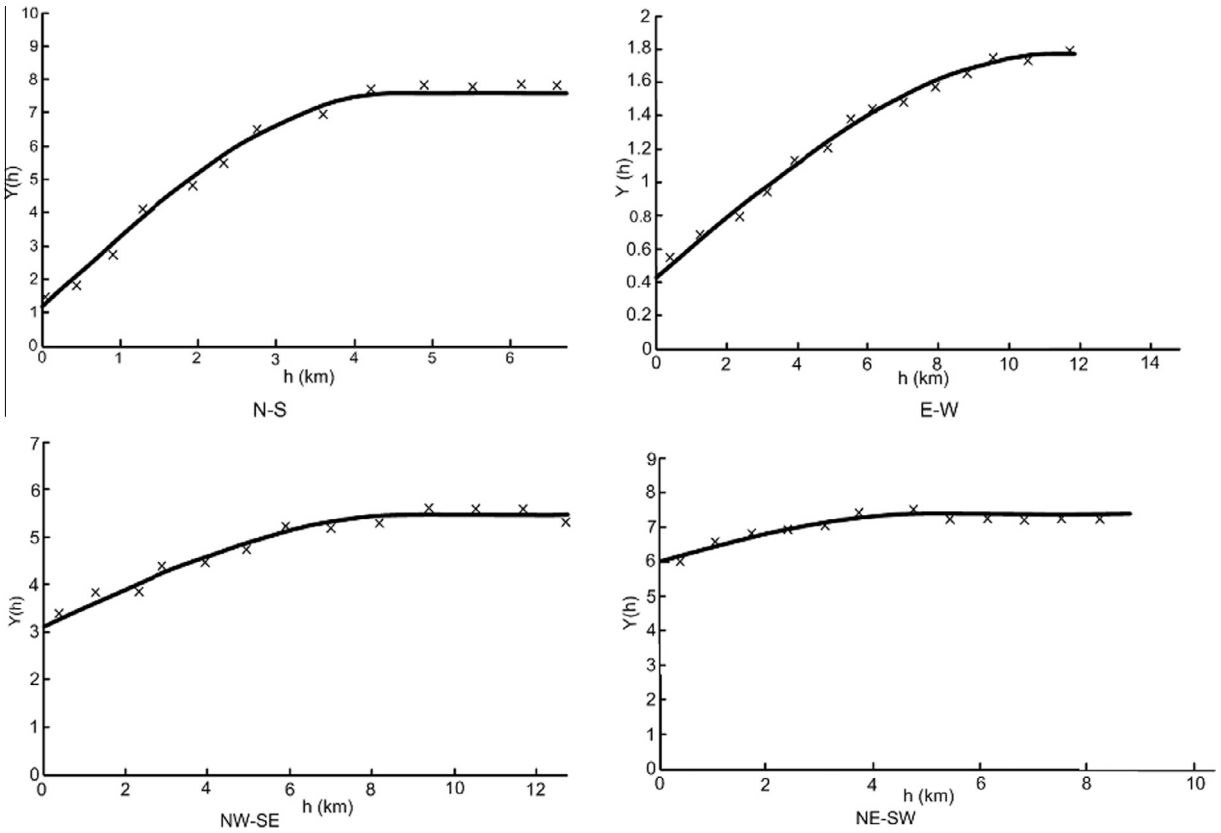

Figure 10 Variogram of the lineaments in direction: (a) N–S, (b) E–W, (c) NW–SE and (d) NE–SW.

Table 3 Regionalisation parameters of lineaments determined from the spherical model.

Direction of lineament	*a* (km)	C_O (km)	$C + C_O$ (km)
N–S	5	1.2	7.6
E–W	11	0.4	1.7
NW–SE	9	3.1	5.4
NE–SW	4	6	7.3
All azimuth	9.6	0.3	7.1

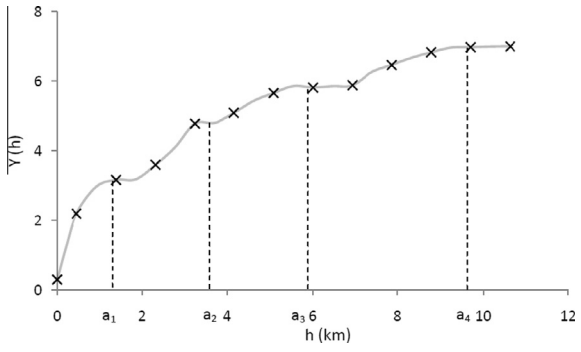

Figure 11 All trends of lineament variogram.

can come from various sources such as measurement errors and the presence of a microstructure associated with a range lower than the distance between two close observations.

The global variogram of lineaments is multi structured with four ranges, determined, respectively at distances$a_1 = 1.6$ km; $a_2 = 3.5$ km; $a_3 = 5.8$ km and $a_4 = 9.6$ km. The maximum range is 9.6 km.

The presence of different parameters in variograms suggests that, the lineaments are spatially structured and the groundwater flow in the crystalline basement, do not occur randomly, but rather in spatially organized manner.

4.4. Confrontation of fracture networks with structural geology

Our work has produced a lineament map of the study area, where we have only few known fractures. It counts hundreds of lineaments of which the reality is strongly probable and which was not known, neither was it even suspected so far. Significant contribution of this map to structural geologists and hydrogeologist adds a new document to verify some of these hypotheses.

The map of the network fractures reveals a high density of discontinuities in all the study area. This density of lineaments gives evidence of tectonic movements which have affected the crystalline base in the course of geological times.

Network analysis of lineament of the study area obtained after analysis of various satellite images, geological maps and field measurement allows highlighting of the orientation of lineaments. The directional lineaments' diagram extracted from the satellite image (Fig. 12a) shows that, a certain group of lineaments stand out from others; that is N0–10; N20–60 and N110–150 which can be regarded as major because they exceed

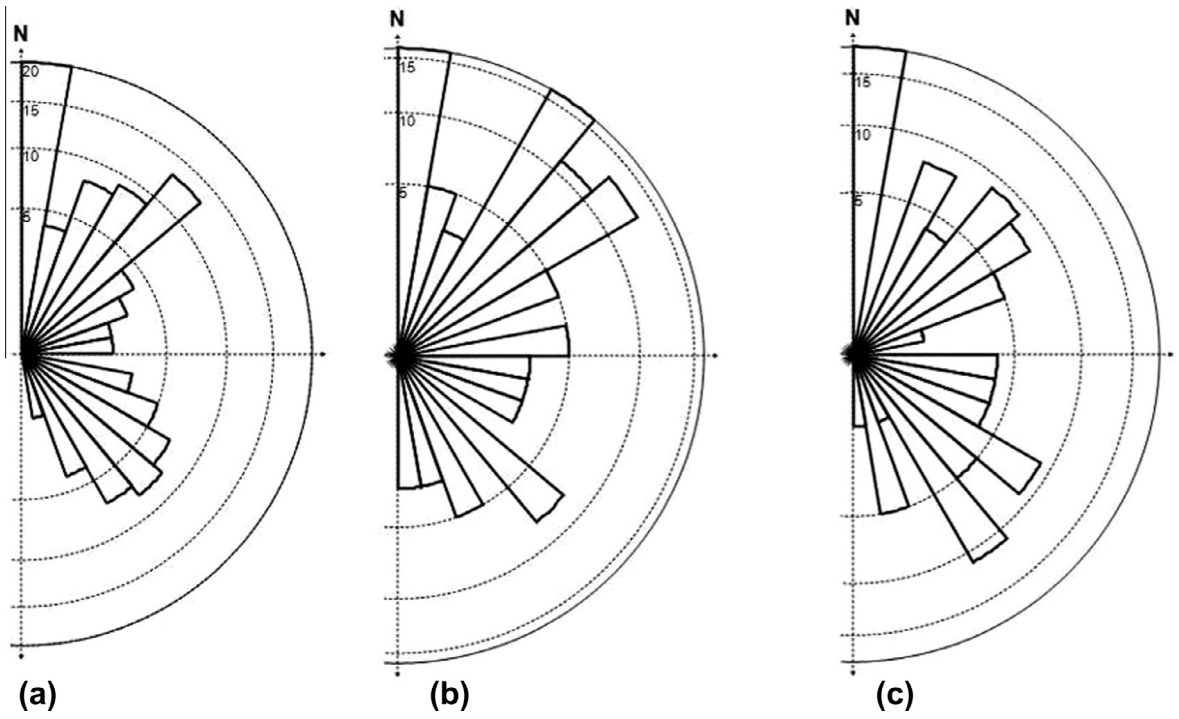

Figure 12 Compass map of: (a) remote sensing lineaments (b) fracturation from the geological map (c) measured lineaments on the outcrop in the study area.

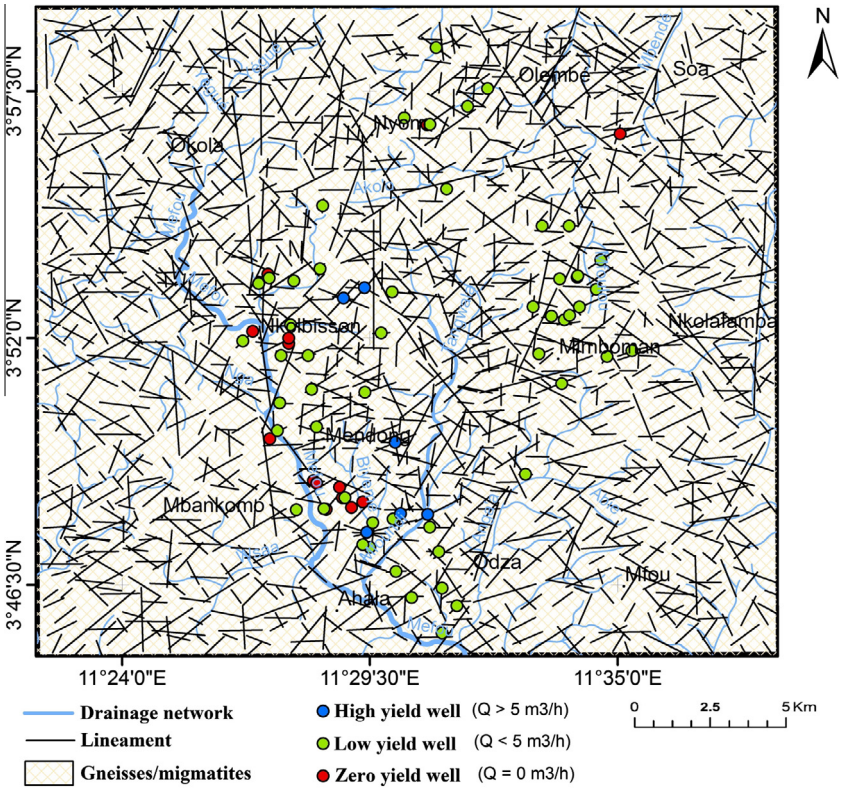

Figure 13 Coupling between maps of lineament obtained from treatment of remote sensing image and location well.

5%. Other groups of lineaments, nearly homogeneous in general can be considered as minor, which are N10–20, N50–110 and N150–180 groups.

Directional lineaments after the geological map (Fig. 12b) show that, the directions N0–10, N30–60 and N130–140 are the most represented. However, classes N70–80; N120–130 and N140–150 are non-existent on the geological map.

Directional lineaments measured on outcrop (Fig. 12c) show that the directions N0–10; N20–30; N40–60; N120–130 and N140–150 are the most numerous. We also note the disparity between N10–20 and N80–90 classes.

The compass card obtained from the detailed map of lineaments from the satellite image, the geological map and the outcrop measurements indicate major lineament directions (N0–10, N20–30, N40–60 and N140–150). The balance between the main directions of lineaments identified on the satellite image, the geological map and the outcrop observations, confirms that the lineaments identified are most likely associated with fracturing. These main orientation NS, NW–SE and NE–SW correspond to the fourth phase of regional deformation compatible with the stress field D3 (Mvondo Ondoa, 2009; Mvondo et al., 2007). These fractures within the post-orogenic relaxation of constraints are reactivated in the neo tectonic context. The deformation of rocks is subjected to a constraint function of the lithology and particularly the orientation of principal stress with respect to the fracture. The opening and closing of fractures are conditioned by the interplay of tectonic movements (compression or decompression).

4.5. Role of lineaments in underground circulations

Coupling of the lineament networks map and the map of spatial repartition of wells is illustrated by Fig 13. This coupling shows a concordance between the two entities. In fact, the different points representing the yield well are aligned to different cartographic lineaments. This result shows that the most important yield obtained in this region are linked to lineaments. On the contrary, zero yields do not present particular organization with respect to lineaments.

It should be noted that, in certain zones where high yield wells have been identified, drilling without yield are present; this tends to demonstrate that productivity of wells is localized and not associated to a stretched base zone, in which underground circulations and productivity are almost generalized (Koita et al., 2010).

In view of high yield exploitation observed at the level of wells, we can retain that these lineaments are hydrologically active. Important yields ($Q > 5\ m^3/h$) were registered at the level of certain lineaments (Fig. 13). These yields were registered onto the group of lineament NW–SE and NE–SW which constitute the groups of lineaments signify interest of the hydrogeological point of view. The fracture nodes and the high fracture sizes are favorable zones for great yield. Research conducted on these fractures becomes a priority in the hydrogeological prospection.

5. Conclusion

This study was conducted to characterize and to analyze the spatial organization of lineaments from SRTM and LTM data using statistical and geostatistical techniques in determining their role in groundwater flow in bedrock aquifers areas. The remote sensing provides a very useful tool for lineament analysis in areas like Yaoundé (Cameroon) where the rock units are not well exposed. The use of different digital image processing algorithms together with controlled field studies allowed extracting and characterizing most of the linear features and their tectonic implications in the study area. Although local variations in trends exist due to the scale of observation, outcrop measurements of lineaments generally reveal orientations similar to those obtained from remote sensing analysis. The geostatistical analysis shows that the lineament network is unambiguously a regionalized variable. The space geometry of these networks does not occur randomly but in a structured and organized manner. This structure is however not isotropic. Finally, the results of the present work could be applicable in the different geologic and environmental aspects based on a good understanding of the genetic and spatial relationships of lineaments systems. These aspects encompass exploration for mineralization and groundwater

Conflict of interest

No conflict of interest.

Acknowledgments

The authors are thankful to the University of Yaoundé I and National Institute of Cartography of Cameroon for providing the necessary facilities to carry out this work. The authors also thank the reviewers for their comments that improved the quality of this paper.

References

Abou El-Magd, I., Hermas, E., El-Bastawesy, M., 2010. GIS-modeling of the spatial variability of flash flood hazard in Abu Dabbab catchment, Red Sea Region, Egypt. Egypt. J. Remote Sens. Space Sci. 13, 81–88.

Akame, J.M., Mvondo-ondoa, J., Olinga, J.B., Essono, J., Mbih, P. K., 2013. Application of (MNT) SRTM numeric field models for mapping structural lineaments: application to the Mezesse Archean, East of Sangmélima (South Cameroon). Geo-Eco-Trop 37, 71–80.

Akame, J.M., Mvondo Ondoa, J., Teikeu, A.W., Owona, S., Olinga, J.B., Messi Ottou, E.J., Ntomba, S., 2014. Apport des Images Landsat-7 ETM+ a l'etude structurale du socle archeen de sangmelima (sud cameroun). Revue Française de Photogrammétrie et de Télédétection 206, 15–26.

Bodin, J., Razack, M., 1999. L'analyse d'images appliquée au traitement automatique de champs de fractures. Propriétés géométriques et lois d'échelle. Bull. Soci. Géol. Fr. 170 (4), 579–593.

Chaabouni, R., Bouaziz, S., Peresson, H., Wolfgang, J., 2012. Lineament analysis of South Jenein Area (Southern Tunisia) using remote sensing data and geographic information system. Egypt. J. Remote Sens. Space Sci. 15, 197–206.

Champetier De Ribes, G., Aubargue, M., 1956. Carte géologique de réconnaissance du Cameroun à 1/500 000, feuille Yaoundé-E. Direction des Mines et de la Géologie du Cameroun.

Chilès, J.P., de marsily, G., 1993. Stochastic models of fracture systems and their use in flow and transport modeling. In: Bear, J., de Marsily, G., Tsang, C.F. (Eds.), Flow and Contaminant

Transport in Fractured Rock. Academic Press, San Diego, California, pp. 169–236.
Chilès, J.P., Guérin, F., Billaux, D., 1992. 3D stochastic simulation of fracture network and flow at Strip a conditioned on observed fractures and calibrated on measured flow rates. In: Tillerson, J.R., Wawersik, W.R. (Eds.), Rock Mechanics. Balkema, Rotterdam, Netherlands, pp. 533–542.
Corgne, S., Magagi, R., Yergeau, M., Sylla, D., 2010. An integrated approach to hydro-geological lineament mapping of a semi-arid region of West Africa using Radarsat-1 and GIS. Remote Sens. Environ. 114, 1863–1875.
Farina, P., Catani, F., Colombo, D., Fumagalli, A., Kukavicic, M., Marks, F., Moretti, S., 2005. Remote sensing: a tool for landslide investigations at a basin scale. Geophys. Res. Abstr. 7, 10157–10168.
Fashae, O.A., Tijani, M.N., Talabi, A.O., Adedeji, O.I., 2014. Delineation of groundwater potential zones in the crystalline basement terrain of SW-Nigeria: an integrated GIS and remote sensing approach. Appl. Water Sci. 4 (1), 19–38.
Goovaerts, P., 2000. Geostatistical approaches for incorporating elevation into the spatial interpolation of rainfall. J. Hydrol. 228, 113–129.
Koike, K., Nagano, S., Kawaba, K., 1998. Construction and analysis of interpreted fracture planes through combination of satellite-image derived lineaments and digital elevation model data. Comput. Geosci. 24 (6), 573–583.
Koita, M., Jourde, H., Ruelland, D., Koffi, K., Pistre, S., Savane, I., 2010. Mapping regional discontinuities and identification of their role in underground hydrodynamics in a base zone: case study of the Dimbokro-Bongouanou region, Ivory Coast. Hydrol. Sci. J. 55, 805–820.
Lasm, T., Razack, M., 2001. Scaling laws in crystalline hard rock fracturing and in the associated river network. C. R. Geosci. 333, 225–232.
Lasm, T., Youan Ta, M., Jourda, P., Kouamé, F.K., 2008. Fracture networks analysis in crystalline basement: case of Bondoukou area (Northeast Cote d'ivoire). Eur. J. Sci. Res. 21, 196–208.
Masoud, A., Koike, K., 2006. Tectonic architecture through Landsat-7 ETM + /SRTM DEM-derived lineaments and relationship to the hydrogeologic setting in Siwa region, NW Egypt. J. Afr. Earth Sci. 45, 467–477.
Meli'i, J.L., Bisso, D., Njandjock, N.P., Ndougsa-Mbarga, T., Banga, F.A., Manguelé-Dicoum, E., 2013. Water-table control using ordinary Kriging in the Southern part of Cameroon. J. Appl. Sci. 13, 393–400.
Michaela, F., Mohamed, G.A., Nicolas, B., 2006. Remote sensing applications to geological problems in Africa. J. Afr. Earth Sci. 44 (2), 7–10.
Moukana, A.J., Koike, K., 2008. Geostatistical model for correlating declining groundwater levels with changes in land cover detected from analyses of satellite images. Comput. Geosci. 34, 1527–1540.
Mvondo, H., Den Brok, S.W.J., Mvondo Ondoa, J., 2003. Evidence for symmetric extension and exhumation of the Yaounde nappe (Pan-African fold belt, Cameroon). J. Afr. Earth Sci. 36, 215–231.
Mvondo, H., Mvondo Ondoa, J., Essono, J., 2007. Tectonic evolution of the Yaoundé segment of the Neoproterozoic central African Orogenic Belt in southern Cameroon. Can. J. Earth Sci. 43, 433–444.
Mvondo Ondoa, J., 2009. Caractérisation des évènements tectoniques dans le domaine sud de la chaine panafricaine au cameroun: styles tectoniques et géochronologies des séries de Yaoundé et Bafia (Thèse Doc). Etat Univ, Yaoundé I, Cameroon, 209P.
Ngnotué, T., Nzenti, J.P., Barbey, P., Tchoua, F.M., 2000. The Ntui Betamba high-grade gneisses: a nordward extension of the Pan African Yaoundé gneisses in Cameroon. J. Afr. Earth Sci. 31, 369–381.
Ngon-Ngon, G.F., Yongue-Fouateu, R., Bitom, D.L., Bilong, P., 2009. A geological study of clayey laterite and clayey hydromorphic material of the region of Yaoundé (Cameroon): a prerequisite for local material promotion. J. Afr. Earth Sci. 55, 69–78.
Njandjock, N.P., Kenfack, C., Diab, A.D., Njeudjang, K., Meli'i, J.L., Kamseu, R., 2013. A geostatistical re-interpretation of gravity surveys in the Yagoua, Cameroon region. Geofis. Int. 52, 365–373.
Nzenti, J.P., 1998. Neoproterozoic alkaline meta-igneous rocks from the Pan-african North Equatorial Fold Belt (Yaounde, Cameroon) biotites and magnetite rich pyroxenites. J. Afr. Earth Sci. 26, 37–47.
Nzenti, J.P., Barbey, P., Macaudière, J., Soba, D., 1988. Origin and evolution of the late precambrian high-grade Yaounde gneisses (Cameroon). Precambrian Res. 38, 91–109.
Owona, S., Mvondo Ondoa, J., Ratschbacher, L., Mbola Ndzana, S. P., Tchoua, M.F., Ekodeck, G.E., 2011. The geometry of the Archean, Paleo and Neoproterozoic tectonics in the Southwest Cameroon. C. R. Geosci. 343, 312–322.
Rashid, M., Lone, M.A., Ahmed, S., 2012. Integrating geospatial and ground geophysical information as guidelines for groundwater potential zones in hard rock terrains of south India. Environ. Monit. Assess. 184 (8), 4829–4839.
Singh, P., Thakur, K.J., Kumar, S., 2013. Delineating groundwater potential zones in a hard-rock terrain using geospatial tool. Hydrol. Sci. J. 58, 213–223.
Tanawa, E., Djeuda Tchapnga, H.B., Ngnikam, E., Temgoua, E., Siakeu, J., 2002. Habitat and protection of water resources in suburban areas in Africa cities. Build. Environ. 37 (3), 269–275.
Tarek, A.S., 2013. Analysis and tectonic implication of DEM-derived structural lineaments, Sinai Peninsula, Egypt. Int. J. Geosci. 4, 183–201.
Teikeu, A.W., Njandjock, N.P., Bisso, D., Yene Atangana, Q., Sep Nlomgan, J.P., 2012a. Hydrogeophysical parameters estimation for aquifer characterisation in hard rock environment: a case study from Yaounde, Cameroon. J. Water Resour. Prot. 3, 244–253.
Teikeu, A.W., Ndougsa-Mbarga, T., Njandjock, N.P., Tabod, C.T., 2012b. Geoelectric investigation for groundwater exploration in Yaoundé area, Cameroon. Int. J. Geosci. 3, 640–649.
Yesou, H., Poin, J.C., Besnus, Y., Saint Jean, R., 1993. Amélioration des données SPOT pour la cartographie structurale en milieu tropical. In: Exemple de la région des chapeaux de fer de Pagala (Togo). Illeme jour. Scient. Res. Télédéct. UREF, Toulouse, 13–16 Novembre 1990, Outils microinformatiques et télédétection de l'évolution des milieux, Presse Univ. Québec, Canada (Ed. PUQ/AUPELF URE), pp. 143–164.